

Simultaneous normal and shear measurements of nanoconfined liquids in a fiber-based atomic force microscope

George Matei,¹ Steve Jeffery,² Shivprasad Patil,¹ Shah H. Khan,¹ Mircea Pantea,¹ John B. Pethica,² and Peter M. Hoffmann^{1,a)}

¹*Department of Physics, Wayne State University, 666 W. Hancock, Detroit Michigan 48201, USA*

²*Department of Materials, University of Oxford, Parks Road, Oxford OX1 3PH, United Kingdom*

(Received 22 August 2007; accepted 14 January 2008; published online 15 February 2008)

We have developed an atomic force microscopy (AFM) technique that can perform simultaneous normal and shear stiffness measurements of nanoconfined liquids with angstrom-range amplitudes. The AFM technique is based on a fiber-interferometric, small-amplitude, off-resonance AFM. This AFM is capable of providing linear quasistatic measurements of the local mechanical properties of confined liquid layers while only minimally disturbing the layers themselves. A detailed analysis of the measurement geometry reveals that shear stiffness measurements are extremely challenging, as even small deviations from perfect orthogonality can lead to data that is very difficult to interpret. We will show ways out of this dilemma and present results that show simultaneous measurement of the shear and normal stiffness of confined liquid layers. © 2008 American Institute of Physics.
[DOI: 10.1063/1.2839913]

I. INTRODUCTION

When a liquid is confined by solid surfaces to spaces of molecular dimensions, its properties differ significantly from those of the liquid in the bulk. In particular, a simple inert liquid with spherical molecules orders itself in layers parallel to the surface of the confining substrates. This structure and its dynamics has been of increasing interest primarily aimed at understanding interfacial phenomena from cell membranes to nanotribology.¹ Geometrically induced layering has been observed by a variety of instruments and experimental techniques such as surface force apparatus,^{2,3} atomic force microscopy,⁴ and new spectroscopic techniques⁵ including fluorescence correlation spectroscopy.^{6,7}

From molecular packing arguments, we would expect that whenever the distance between the confining surfaces is an integer number of the respective molecular size, the layering of the molecules is in a high density state. At other separations, molecular packing is disrupted and the liquid assumes a low density state. However, within the confining gap, the density is not uniform and the above statements hold true only for the average density across the gap.⁸ There may also be significant fluctuations in the density of the confined liquid, complicating the simple quasistatic geometric model of the confined liquids.⁵ Moreover, there is a long-standing debate on the dynamics of these systems between those claiming crystallization, glass formation, or no transition upon confinement.^{9,10} Yet, another recent report¹¹ shows that a confined liquid can behave like a Newtonian liquid with little change in its dynamics or a pseudosolid, depending on the rate of approach of the confining surfaces. Clearly, the behavior of liquids confined at molecular scales is rather complex and there is, hence, a great need for developing new

AFM-based techniques to further improve understanding in this area. In particular, the question if the liquid behaves as a solid or liquid is more clearly resolvable, if the shear stiffness of the liquid is measured, rather than the stiffness in the normal direction. The normal stiffness is more influenced by the substrate and squeeze-out dynamics. Moreover, it is of interest how the observed normal and lateral stiffnesses are related, especially in light of the recent discovery of kinetically induced changes in the nanomechanics of the confined liquid.¹¹ Other areas where such simultaneous measurements of mechanical properties in two independent directions are important include polymer films, lipid bilayers and cell membranes, dimerization of membrane proteins, or layered solid materials.

In this paper, the development of a new AFM technique for *simultaneous* normal and shear stiffness measurements in the linear regime is presented. The unique aspect of the presented work is that we are measuring the shear stiffness in the small-amplitude regime, i.e., prior to slip. This allows us to probe the equilibrium mechanical state of the liquid and the transition to any nonequilibrium states induced by squeezing or sliding.¹¹ Here, “small amplitudes” refer to free lateral and normal amplitudes that are less than one molecular diameter. Such measurements require high sensitivity, as well as special precautions and a thorough analysis of the measurement conditions. We will discuss experimental constraints and provide guidance to design experiments that provide optimal separation of shear and normal stiffness measurements in the small-amplitude regime. Measurements of confined tetrakis (2-ethylhexoxy) silane (TEHOS) and octamethylcyclotetrasiloxane (OMCTS) layers were performed with a homebuilt (sub-) angstrom amplitude, off-resonance AFM using a fiber-based interferometric sensor.^{12,13} We describe the measurement technique in detail and discuss the results in terms of instrument performance.

^{a)}Electronic mail: hoffmann@wayne.edu.

II. NORMAL AND SHEAR INTERACTION STIFFNESS: THEORETICAL OUTLINE

A. Measurement of the normal sample stiffness

Small-amplitude, off-resonance AFM is a dynamic technique in which the cantilever is vibrated below its resonance at a free amplitude in the angstrom range and its distance-dependent amplitude and phase are measured. Ideally, such amplitudes are small enough so that the total force between tip and sample is linear over the trajectory of the tip.¹⁴ In this case, the amplitude and phase of the cantilever motion can be directly related to the local interaction stiffness in the normal (vertical) direction, k_n , and energy dissipation or damping coefficient C . It has been shown^{14,15} that the use of small amplitudes allows linear measurements of any force field as long as amplitudes are sufficiently small and allows solving the equation of motion in a simple, closed form. Hence, the normal interaction stiffness and damping coefficient can be mapped point by point with this technique. Moreover, the use of small amplitudes allows for a minimally perturbative measurement of local mechanical properties and thus other dynamics effects, such as the influence of squeeze rate, can be measured without disturbance from the oscillating cantilever.¹¹

In our measurements, we measure the amplitude and phase (between the piezodrive and the cantilever end) at an oscillation frequency far below the first resonance of the cantilever, typically in the 100–1000 Hz range. For the normal oscillations of the cantilever, using the small-amplitude approximation in the equation of motion of the cantilever, we then find

$$k_n = k_L \left(\frac{A_{n0}}{A_n} \cos \varphi - 1 \right) \quad (1)$$

and

$$C = - \frac{k_L A_{n0}}{A_n \omega} \sin \varphi. \quad (2)$$

Here, A_{n0} is the free normal amplitude, A_n is the measured amplitude as the surface is approached, φ is the measured phase of the cantilever, and ω its drive frequency. If the AFM is operated far below the resonance, the phase angle is close to zero and Eq. (1) becomes

$$k_n = k_L \left(\frac{A_{n0}}{A_n} - 1 \right). \quad (3)$$

The above result can also be obtained if, close to the surface, the cantilever and normal interaction stiffness are considered as two springs in series and in equilibrium, subject to the same force,

$$F = k_n A_n = k_L (A_{n0} - A_n). \quad (4)$$

This assumption is justified in the subresonance regime, when the measurement becomes quasistatic.

B. Shear measurements and influence of angular misalignment

In the previous discussion, we calculated the motion of the cantilever assuming that the orientation and motion of the

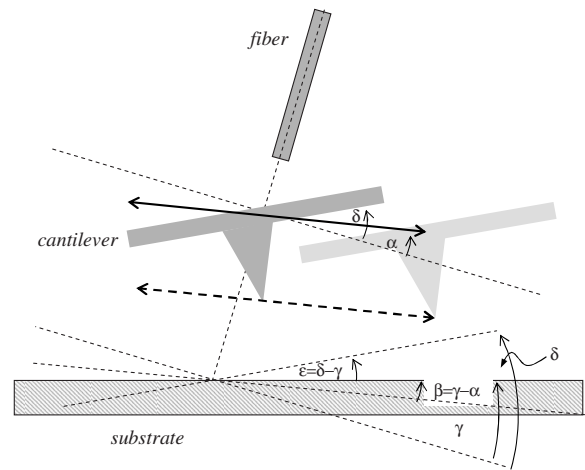


FIG. 1. Schematic showing relevant angles associated with the translational motion of the cantilever during measurement. Angles are referenced either to the fiber end or the substrate surface. α is the angle between the fiber end and the direction of translational motion of the cantilever, while β is the angle between the motion of the cantilever and the substrate surface. γ is the angle between the fiber end and the substrate surface and δ is the angle between the fiber end and the cantilever surface. ϵ is the angle between the cantilever surface and the substrate surface. The double arrows denote the direction of the oscillatory translational motion of the cantilever.

cantilever is perfectly aligned with the sample surface. However, in a real experiment, it is not always possible to perfectly align the system. Instead, there will always be small misalignment angles. Since our goal is to neatly separate normal and lateral stiffness values in a simultaneous measurement, a careful analysis of the effect of the angular misalignment is needed. It turns out that for measurements in the *normal* direction, the above derived expressions hold to a good degree of accuracy. However, the story is quite different for measurements of the shear stiffness of the liquid.

In the following, we will develop a general theory of cantilever motion, while restricting ourselves to the following assumptions: (1) the cantilever is oscillated at very small amplitudes (0.1–2 nm). This implies that over the oscillation period, the normal and lateral stiffness of the liquid are constant. Furthermore, in this regime, tip translations and rotations (torsion) can be separately treated, as any cross terms would be second order in the already very small amplitudes. (2) The AFM will be operated well below its first resonance. This implies that inertial and damping terms can be for the most part neglected (or at least will not overly influence our conclusions). As we will see, even with these simplifying assumptions, the full analysis of the cantilever motion in the linear, quasistatic regime presented here is challenging. (3) As the cantilever is oscillated and measured at the frequency of oscillation, we are only interested in changes of the lever position and bending, not in any static deformations.

Figure 1 shows a schematic of the angles we need to consider in this problem, assuming that it is sufficient to consider angles in the plane of the shear motion only. Since in our case we are using a fiber-interferometric system, all the angles are referenced to the orientation of the fiber end (dashed line) or the substrate surface. Angle α is the angle between the fiber end and the direction of motion of the cantilever end (solid double arrow), while δ is the angle be-

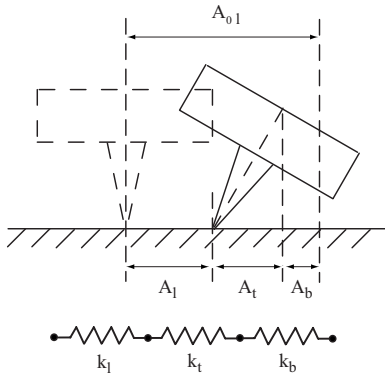


FIG. 2. Schematic showing the response of the cantilever to a pure shear motion. The lateral motion of the base A_{0l} is accommodated by lateral bending and torsion of the cantilever (A_b and A_t , respectively), and lateral deformation of the tip-surface contact (A_l).

tween the cantilever surface (assumed to be perpendicular to the tip) and the fiber end. Note that α and δ do not have to be identical. While the former is mostly determined by the piezomotion, the latter is mostly determined by how the cantilever is mounted on the holder. Moreover, both angles can change when the tip interacts with the surrounding liquid and the substrate. The angle between the fiber end and the surface is denoted by γ and is the only angle in this problem that is assumed to not depend on the tip-surface interaction and is therefore fixed. The angle between the substrate surface and the direction of motion of the cantilever is given by $\beta = \gamma - \alpha$ and the angle between the cantilever surface and the substrate surface is $\epsilon = \delta - \gamma$. We can now analyze the motion of the cantilever and the resulting interferometric measurement of that motion as a function of these angles.

By separating the translational and rotational motions (torsion or twist) of the tip, we can initially restrict our considerations to the translational motion only. However, we need to keep in mind that some of the force will be taken up by the cantilever torsion. The torsional motion is due to a torque applied along the length of the tip and is therefore perpendicular to the tip. Let us assume that the cantilever base is moved sideways (perpendicular to the tip) by some distance A_{0l} by a shear piezo. Part of this motion will move the tip sideways by a distance A_l . If there is a finite lateral sample stiffness k_l , some of the lateral motion will be accommodated by the cantilever through sideways bending (A_b) and torsion (A_t), as shown in Fig. 2. Thus, the total lateral motion is given by

$$A_{0l} = A_l + A_t + A_b. \quad (5)$$

Since the corresponding spring constants are in series, the force in each spring will be the same,

$$F = k_l A_l = k_t A_t = k_b A_b. \quad (6)$$

Solving these equations for the translational motion of the tip, A_l , we find

$$A_l = \frac{A_{0l}}{1 + k_l/k_{bt}}, \quad (7)$$

where $k_{bt} = k_b k_t / (k_b + k_t)$ is an effective lateral stiffness of the cantilever. We can also use these equations to determine the

shear stiffness of the sample, k_l , assuming we can measure A_{0l} and A_l ,

$$k_l = \frac{A_l k_t k_b}{A_{0l} k_b - A_l (k_b + k_t)}. \quad (8)$$

In order to consider the translational motion of the lever subject to the lateral and normal stiffness of the lever, we will use a coordinate system that is oriented with the x and z along the substrate surface and the y perpendicular to it. Then, if A_0 is the applied cantilever amplitude and β_0 is the initial angle between this amplitude and the substrate surface, the vertical (normal) and lateral (shear) components of the piezomotion (motion of the cantilever base) are

$$A_{n0} = A_0 \sin \beta_0, \quad (9a)$$

$$A_{l0} = A_0 \cos \beta_0. \quad (9b)$$

Similar equations apply to the motion of the tip where A_0 is replaced by A and β_0 is replaced by β .

From Eq. (4), we recall that in the quasistatic, linear regime, the amplitude of the cantilever can be obtained from a force balance. We will derive an analogous equation for the general case, where the tip is oriented in some arbitrary orientation with respect to the sample and is oscillated in some direction that is not necessarily in line with either the cantilever or the sample. The corresponding angles are shown in Fig. 1. In this case, the forces and amplitudes will be vectors and correspondingly, the stiffnesses have to be represented by tensors, analogous to a stress-strain relationship in an anisotropic material.

For the tip-sample interaction, there are two relevant stiffnesses: k_l and k_n . These can be regarded as springs acting in the orthogonal x and y directions, respectively. The cantilever can also be represented by two orthogonal stiffnesses, k_L and k_{bt} . However, these are acting in directions which are rotated by an angle ϵ with respect to the substrate. Thus, the master equation describing the force balance (and the amplitudes in the quasistatic, linear regime) should be written as

$$\mathbf{K}_{ts} \mathbf{a} = \mathbf{R} \mathbf{K}_L \mathbf{R}^T (\mathbf{a}_0 - \mathbf{a}). \quad (10)$$

Here, $\mathbf{a} = (A_l, A_n, 0)^T$ is the vector describing the tip motion, while $\mathbf{a}_0 = (A_{l0}, A_{n0}, 0)^T$ is the vector describing the motion of the cantilever base, i.e., the motion imposed on the cantilever by the drive piezo(s). \mathbf{K}_{ts} is the elastic tensor of the tip-surface interaction, given by

$$\mathbf{K}_{ts} = \begin{pmatrix} k_l & 0 & 0 \\ 0 & k_n & 0 \\ 0 & 0 & k_l \end{pmatrix}. \quad (11)$$

\mathbf{K}_L is the elastic tensor of the cantilever, given by

$$\mathbf{K}_L = \begin{pmatrix} k_L & 0 & 0 \\ 0 & k_{bt} & 0 \\ 0 & 0 & k_c \end{pmatrix}. \quad (12)$$

Here, $k_c \gg k_L, k_{bt}$ is included for completeness, but it will not play a role in the calculations, because the translation of the tip is restricted to the x - y plane. As noted above, the cantilever and tip are rotated with respect to the substrate-

centered coordinate system. This is represented by the rotation matrix \mathbf{R} , which is given by

$$\mathbf{R} = \begin{pmatrix} \cos \epsilon & -\sin \epsilon & 0 \\ \sin \epsilon & \cos \epsilon & 0 \\ 0 & 0 & 1 \end{pmatrix}. \quad (13)$$

Multiplying out all the terms in Eq. (10) leads to the following full equations, describing the force balance in the x - y plane:

$$k_t A_l = k_L \{-\sin \epsilon [\sin \epsilon (A_{0l} - A_l) + \cos \epsilon (A_{0n} - A_n)]\} \\ + k_{bt} \{\cos \epsilon [\cos \epsilon (A_{0l} - A_l) + \sin \epsilon (A_{0n} - A_n)]\}, \quad (14a)$$

$$k_n A_n = k_L \{\cos \epsilon [\sin \epsilon (A_{0l} - A_l) + \cos \epsilon (A_{0n} - A_n)]\} \\ + k_{bt} \{\sin \epsilon [\cos \epsilon (A_{0l} - A_l) + \sin \epsilon (A_{0n} - A_n)]\}. \quad (14b)$$

Although these equations can be, in principle, solved for A_l and A_n , it is easier to consider some special cases. If the tip is perfectly aligned with the surface, $\epsilon=0$, and we obtain

$$k_t A_l = k_{bt} (A_{0l} - A_l), \quad (15a)$$

$$k_n A_n = k_L (A_{0n} - A_n). \quad (15b)$$

This recovers Eqs. (7) and (4), and the two directions are perfectly separated. In reality, however, it is very difficult to ensure that the angle ϵ is equal to zero. Thus, we have to consider the possibility that there is a small misalignment $\epsilon \neq 0$, but with $\epsilon \ll 1$. In this case, we will only consider terms that are first order in ϵ and use $\cos \epsilon \approx 1$ and $\sin \epsilon \approx \epsilon$. In this limit, we find after solving for A_l and A_n ,

$$A_l = \frac{A_{0l}}{1 + k_t/k_{bt}} + \epsilon \frac{k_{bt} - k_L}{(k_t + k_{bt})(k_n + k_L)} k_n A_{0n}, \quad (16a)$$

$$A_n = \frac{A_{0n}}{1 + k_n/k_L} + \epsilon \frac{k_{bt} + k_L}{(k_t + k_{bt})(k_n + k_L)} k_t A_{0l}. \quad (16b)$$

The first term on the right-hand side of each equation represents the well-separated contribution, while the second term describes the undesired cross-talk contribution. Although the cross-talk terms are scaled by ϵ , they can be significant, depending in the values of the elastic constants. The total amplitude of the tip is given by $A = \sqrt{A_l^2 + A_n^2}$ and the angle of the tip motion with respect to the substrate is given by $\tan \beta = A_n/A_l$. Note that this angle is not necessarily the same as β_0 , which is the angle imposed by the piezodrive.

The discussion so far is valid for any AFM, independent of the mechanism of deflection measurement. In our case, the motion of the cantilever is measured by a single optical fiber interferometer, located at some off-axis position on top of the cantilever, as shown in Fig. 3. To calculate what the fiber measures, we now need to take the angles α and δ into account. The fiber will measure any amplitude that is perpendicular to the fiber end (i.e., moving toward or away from the fiber) but not detect any amplitude parallel to the fiber. If A is

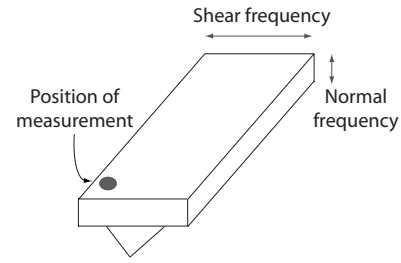


FIG. 3. Simultaneous normal and torsional amplitude measurements are performed with a single fiber positioned close to the edge of the cantilever. Both the vertical and torsional motions of the tip result in a vertical displacement at the point of measurement separated in the frequency domain.

the amplitude at which the cantilever end moves by translation (i.e., with $\delta = \text{const.}$), we find that the fiber detects an amplitude A_m , given by

$$A_m = A(\sin \alpha - \cos \alpha \tan \delta). \quad (17)$$

We immediately notice is that if $\alpha = \delta$, $A_m = 0$. In this case, the motion of the cantilever end is parallel to the cantilever surface and therefore the cantilever surface moves such that the distance of the surface to the fiber end is unchanged. In this situation, the fiber will not measure any translational motion of the tip. To align the cantilever motion in this way initially (far from the surface) is desirable, as this minimizes cross-talk between the lateral and normal motions of the cantilever and maximizes sensitivity to the torsional motion of the cantilever. Such an alignment can be achieved by using two perpendicular piezos, connected through a compensation circuit as described below.

So far, we have only considered translational motions of the cantilever and tip. Now, we will add the torsional motion of the cantilever, which leads to a rotation of the cantilever end and the tip. As we are only interested in a *change* of the tilt angle, the relevant force is given by the left-hand side of Eq. (10). This force $\mathbf{F} = (k_t A_l, k_n A_n, 0)^T$ acts on the tip end and causes a torque $\boldsymbol{\tau}$. Again, we consider the mechanical equilibrium situation (something we can do in the quasistatic regime under discussion here). We find

$$\boldsymbol{\tau} = |\mathbf{h} \times \mathbf{F}| = k_\theta \theta. \quad (18)$$

Here, $\theta \approx \tan \theta \approx A_t/h$ is the small twist angle due to the applied torque. $k_\theta = h^2 k_t$ is the angular torsional stiffness of the lever, and \mathbf{h} is a vector representing the tip with length h and pointing in the direction of the tip:

$$\mathbf{h} = (h \sin \epsilon, -h \cos \epsilon, 0)^T. \quad (19)$$

Note that $\epsilon = \epsilon_0 + \theta$, where ϵ_0 is the initial tilt angle of the lever before twisting. Substituting for ϵ and using that fact that θ is small, we can solve for θ :

$$\theta = \frac{k_n A_n \sin \epsilon_0 + k_t A_l \cos \epsilon_0}{k_t A_l \sin \epsilon_0 - k_n A_n + k_t h}. \quad (20)$$

In the case of perfect alignment ($\epsilon = \beta = 0$), we obtain $\theta = k_t A_l / k_t h = A_l/h$ as before [compare Eq. (6)].

This calculation of the lever torsion is also quite general and independent of the measurement sensor. The lateral sections of the sectioned photodiode in a laser deflection AFM are sensitive to the tilt angle only and not to the translational

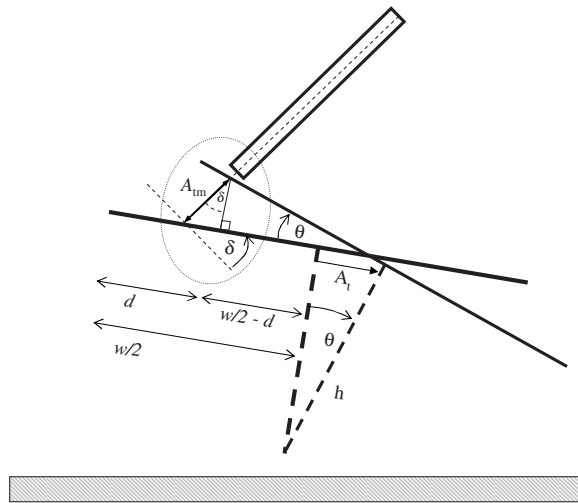


FIG. 4. Schematic showing relevant angles associated with the torsional motion of the cantilever. The torsional angle is θ , which leads to a change of the lever angle δ . w is the width of the cantilever and d is the position of fiber along the lever. A_l is the laterally measured torsional amplitude, which translates into a measured vertical amplitude A_{tm} . Note that the angles in this schematic are greatly exaggerated for clarity. In an experiment, the position of the fiber will remain essentially unchanged as typical torsional angles are in the $<10 \mu\text{rad}$ range.

motion of the cantilever. This can be an advantage compared to our fiber-interferometric system, which is sensitive to both the translational and torsional motions of the cantilever. However, even the torsional motion is prone to cross-talk as Eq. (20) shows.

Now, we will determine what the fiber measures due to the torsional motion of the lever. To be complete, we include a possible initial tilt angle δ of the fiber with respect to the cantilever surface. We find by inspection of Fig. 4:

$$A_{tm} = \left(\frac{w/2 - d}{\cos \delta} \right) \theta = \left(\frac{w/2 - d}{h \cos \delta} \right) A_l. \quad (21)$$

The dimensions w and d are indicated in Fig. 4, and correspond to the full width of the cantilever and the location of the laser spot, respectively. Please note that, in Fig. 4, angles are greatly exaggerated for clarity and that it is safe to assume that the laser spot will not move when the cantilever tilts.

Now, we can write down an expression for the total signal measured by the fiber interferometer:

$$A_{m,\text{tot}} = |A_m + A_{tm}|. \quad (22)$$

It should be noted that A_m and A_{tm} can be positive or negative and thus can either add or subtract to produce the total measured signal.

Figure 5 shows examples calculated for a theoretical normal and lateral stiffness profile, based on the above equations. It shows that at high torsional lever stiffness and even slight misalignment angles, severe artifacts can arise in the measurement of the lateral stiffness of the sample. In Fig. 5, the curve with a thick line corresponds to the actual (theoretical) shear stiffness of the liquid, while the other curves are the results of simulated measurements under various conditions. At any torsional stiffness, a measurement at perfect alignment will provide perfect measurement fidelity. How-

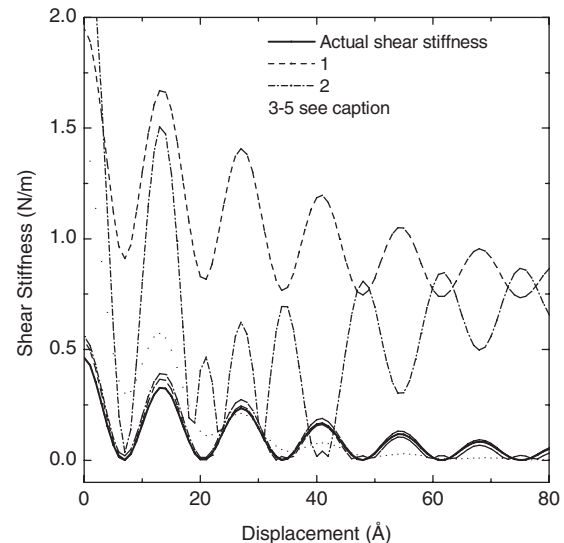


FIG. 5. Simulated shear measurements. The actual (theoretical) shear stiffness is indicated by the thick line. Curve 1 (dashed, top) shows the results of a measurement with a commercial cantilever ($k_t=93 \text{ N/m}$) and a misalignment $\epsilon=-0.5^\circ$ and incomplete compensation $\alpha-\delta=0.25^\circ$. Curve 2 (dash dot, second from top) corresponds to $\epsilon=-1^\circ$ and $\alpha-\delta=-0.3^\circ$. Curve 3 corresponds to a measurement with $\epsilon=\alpha-\delta=0$ and completely overlays the theoretical curve. This is the case of perfect alignment. Curves 4 and 5 (thinner line curves that are very close to theoretical curve) correspond to misaligned measurements using a lever with a highly reduced torsional stiffness of $k_t=2.3 \text{ N/m}$. It can be seen that while there is some deviation from the theoretical curve, the effect of misalignment is in this case greatly reduced.

ever, when a cantilever of high torsional stiffness is used (for example, we used $k_t=93 \text{ N/m}$, for a typical commercial lever in this calculation), even small misalignment angles can cause severe measurement artifacts. Curve 1 (upper curve, dashed) shows a measurement with a lever misaligned by only $\epsilon=-0.5^\circ$ to the substrate and a motion misaligned by $\alpha-\delta=0.25^\circ$ with the cantilever. It shows a large offset and increase of the peak heights, but does at least represent qualitatively the peak positions of the actual stiffness of the liquid. A misalignment corresponding to $\epsilon=-1$ and $\alpha-\delta=-0.3$ gives the measurement shown in the dash-dotted curve (curve 2). This curve is significantly distorted, showing an initial decrease of the stiffness, followed by an increase. It also shows peaks that are offset from the actual stiffness of the liquid, as well as additional half-period peaks. It does, therefore, not even qualitatively resemble the actual stiffness. Finally, we included examples of simulated measurements with the same misalignment, but with a lever that has a torsional stiffness of only 2.3 N/m . In this case, the measurements are very close to the actual stiffness, and the effect of misalignment is greatly reduced. Thus, levers with low torsional stiffnesses are highly desirable.

III. EXPERIMENTAL PROCEDURE

The measurement of changes of much less than 1 \AA in the cantilever amplitude requires a deflection sensor with very high sensitivity. Our homebuilt AFM includes a fiber-optic interferometric sensor that was presented in detail in Ref. 13 and was ultimately based on the design of Rugar *et al.*¹⁶ The alignment of the fiber perpendicular to the can-

tilt is carried out with submicron precision to achieve an enhanced sensitivity based on multiple reflections between the cantilever and the end of the fiber.¹²

Simultaneous normal and torsional cantilever amplitude measurements can be performed with a single fiber by positioning it close to an edge of the cantilever and oscillating the cantilever vertically and laterally at different frequencies, as sketched in Fig. 3. The vertical vibration of the cantilever generates a vertical tip motion and, hence, a vertical displacement at the point of measurement detected by a lock-in amplifier as the normal amplitude. Any change in this amplitude is due to the presence of a normal force gradient between the tip and the sample. On the other hand, as shown above, a lateral vibration of the cantilever generates no vertical displacement at the point of measurement unless the cantilever twists in the presence of a lateral force or there is a misalignment with respect to the fiber. The vertical displacement at the frequency of the lateral motion is detected by a second lock-in amplifier. As both the vertical and lateral motions of the tip result in a vertical displacement at the point of measurement, the two components can be measured with a single fiber provided they are well separated in the frequency domain.

A. Normal and lateral vibration cross-talk compensation

As discussed in detail above, a pure lateral vibration of the cantilever generates no vertical displacement at the point of measurement in the absence of twist or torsion induced by a lateral force field. Any residual amplitude detected at shear frequency when the cantilever is far away from the sample is an indication of cross-talk between the normal and lateral vibration modes of the cantilever. This cross-talk is due to the cantilever tilt angle and any residual normal vibration (expansion and contraction) of the shear piezoactuator at shear frequency. In principle, there could also be cross-talk arising from inertial effects in the surrounding liquid. However, at the small amplitudes and frequencies used in our techniques, the liquid loading can be assumed to be quasi-static and unsteady fluid inertial effects can be neglected.¹⁷

In order to compensate some of these effects, a part of the shear signal can be fed to the dither (normal) piezo and its amplitude can be adjusted until the measured amplitude at the frequency of the lateral motion is nulled far from the surface (Fig. 6). The adjustment of the shear signal amplitude fed to the dither piezo is achieved with a variable resistor while its mixing with the normal signal is performed by a summing operational amplifier. The compensator electronic circuit is shown in Fig. 7.

However, the compensator circuit will only align the lateral cantilever motion with the surface of the cantilever far from the surface ($\alpha_0 - \delta_0 = 0$) and does not align the cantilever and its motion with the substrate. We therefore need to find ways to measure and adjust the alignment of the tip motion with the surface. This can be achieved by performing a surface scan.¹⁸ This works well in larger amplitude measurements (friction measurements), where the lateral motion is provided by the sample scanner. However, in the cases where the lateral motion is provided by a shear piezo with

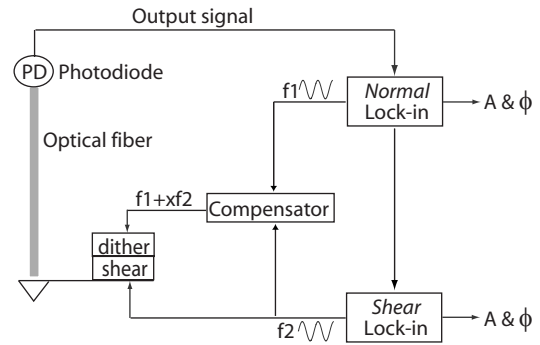


FIG. 6. Schematic of electronic setup for simultaneous normal and shear measurements. A shear oscillation is applied via the shear piezo to the base of the cantilever. A part of this signal is mixed with the normal signal and fed to the dither piezo for cross-talk compensation. The resulting deflection signal, measured by a high-sensitivity fiber interferometer, is split and analyzed by two lock-in amplifiers at the normal and shear frequency components, yielding measurements of normal and shear amplitudes, respectively.

limited travel, we have to resort to other means, such as measuring the alignment of the cantilever chip with the sample using a charge coupled device (CCD) camera. In our case, we were able to do this with a measured accuracy of about 0.5° .

B. Cantilever stiffness calibration

In the case of a uniform rectangular beam of elastic modulus E , width w , thickness t , and length L , the normal bending stiffness is

$$k_L = \frac{Ewt^3}{4L^3}, \quad (23)$$

while its resonance frequency is

$$f = \frac{1}{2\pi L^2} \sqrt{\frac{\alpha^4 E}{12\rho}}, \quad (24)$$

where ρ is the density and α is a numerical constant referring to the first mode of vibration of the beam.^{19,20} The above equations can be combined to eliminate an unknown variable, depending on the preference. If, for instance, Young's modulus is eliminated, the normal stiffness becomes

$$k_L = \frac{12}{\alpha^4} \pi^2 f^2 wtL\rho. \quad (25)$$

Similarly, the lateral bending stiffness of the cantilever can be expressed as

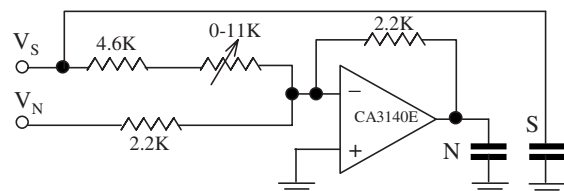


FIG. 7. Compensator electronic circuit. The adjustment of the shear signal amplitude, that is mixed with the normal amplitude signal and fed to the dither piezo, is achieved by a variable resistor. The two signals are mixed by a summing operational amplifier.

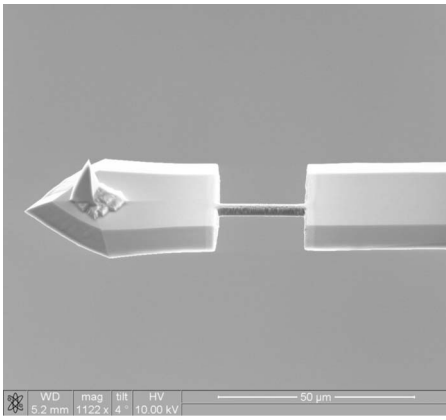


FIG. 8. SEM image of a commercial cantilever micromachined by FIB for enhancement of torsional signal sensitivity.

$$k_b = \frac{Ew^3t}{4L^3}, \quad (26)$$

while the beam torsional bending stiffness can be written in the form

$$k_t = \beta \frac{Gwt^3}{h^2L}, \quad (27)$$

where $G = E/2(1 + \nu)$ is the beam shear modulus, ν is the Poisson ratio, h is the tip length, and β is a constant that can be calculated from a convergent series depending on the (w/t) ratio.^{21–23} The lateral bending and torsional stiffness expressions can be rearranged in terms of the normal bending stiffness of the beam as

$$k_b = \left(\frac{w}{t}\right)^2 k_L \quad (28)$$

and

$$k_t = \frac{2\beta}{1 + \nu} \left(\frac{L}{h_t}\right)^2 k_L. \quad (29)$$

A regular cantilever can generate a torsional signal just above the thermal noise limit, as calculated for our instrument in Ref. 13. In order to enhance the torsional signal sensitivity, the cantilever can be modified to have a lower lateral bending and torsional stiffness. Figure 8 shows a scanning electron microscopy (SEM) image of such a cantilever we obtained by micromachining a commercial cantilever²⁴ by using a focused ion beam (FIB) system. Even more elaborate structures can be used to mechanically fully decouple normal and lateral motions.²⁵

The stiffness values for a modified cantilever can be calculated from beam theory by superposition of the deflections of each section. This is done by calculating the deflection d due to a unit load P and then determine the needed stiffness from $k = P/d$. For the normal and bending stiffnesses, we need to realize that the angle achieved at the end of each section due to its bending leads to an additional deflection along the length of the *next* section, in addition to that section's own bending. We also need to take into account the moment generated by the load at the end of the tip along the

remaining length of the tip, measured from the end of each section.

It can be worked out that for a rectangular beam, with N sections of lengths l_i , widths w_i , and thicknesses t_i , the total bending deflection at the beam end is given by

$$d_{\text{tot}} = \sum_{i=1}^N d_i + \sum_{i=2}^N l_i \left(\sum_{j=1}^{i-1} \phi_j \right). \quad (30)$$

Here, d_i are the individual bending deflections of each section i , while ϕ_j are the additional angles generated at each end of a section by its bending deflection.

The correct equation for the bending deflection of each section is given by

$$d_i = \frac{Pl_i^3}{3EI_i} + \frac{(Px_i)l_i^2}{2EI_i}. \quad (31)$$

Please note that two terms are needed, one for the load applied at the section end by the next section and one for the moment applied along the remaining lever length. Here, x_i is the length over which the moment Fx_i is applied, i.e., the remaining length along the cantilever measured from the end of the respective section. It is given by

$$x_i = \begin{cases} \sum_{j=i+1}^N l_j & \text{if } i < N \\ 0 & \text{if } i = N. \end{cases} \quad (32)$$

The I_i 's are the appropriate area moments, given by

$$I_{v,i} = \frac{wt^3}{12}, \quad (33a)$$

$$I_{l,i} = \frac{w^3t}{12}. \quad (33b)$$

The first one is the vertical moment, which should be used when calculating vertical deflections (and thus k_L), while the second expression is to be used for lateral bending (k_b). Finally, the correct expression for the appropriate bending angles is

$$\phi_j = \frac{Pl_j^2}{2EI_j} + \frac{(Px_j)l_j}{EI_j}. \quad (34)$$

Although this seems quite complicated, these expression collapse to expressions (23) and (26) if all the sections have identical w and t .

For the torsional stiffness of a sectioned lever, we can simply add the twist angles of each section, i.e., $\theta_{\text{tot}} = \sum_{i=1}^N \theta_i$. The individual twist angles are given by

$$\theta_i = \frac{\tau l_i}{J_i G}. \quad (35)$$

Here $\tau = Ph$ is the applied torque (h is the length of the tip) and J_i is the torsional constant of section i , given by²⁶

$$J_i = \frac{w_i t_i^3}{3} \left(1 - 0.63 \frac{t_i}{w_i} \right). \quad (36)$$

Note that J_i is *not* identical to the so-called polar area moment, which can be found by adding $I_{v,i}$ and $I_{l,i}$. This is a

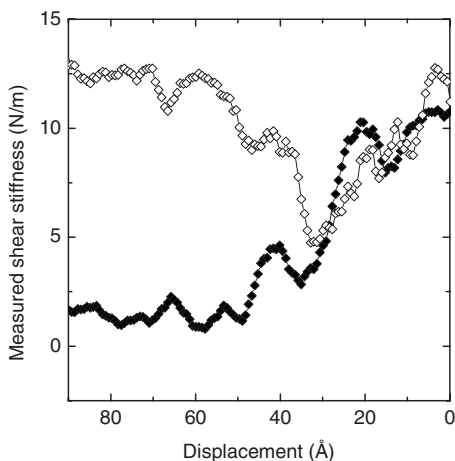


FIG. 9. Measurement of the shear stiffness of nanconfined TEHOS with (filled symbols) and without (open symbols) compensator circuit. Without compensator circuit, the shear stiffness has unphysically high values far from the surface due to the measurement of the misaligned translational motion of the cantilever. Both measurements show stiffness oscillations consistent with the size of the molecules.

common mistake and can lead to misjudging the torsional stiffness of the levers by orders of magnitude. The torsional angular stiffness can now be found from $k_\theta = \tau / \theta_{\text{tot}}$. This can be converted to the k_t by $k_t = k_\theta / h^2$.

C. Materials and measurement methods

We have previously reported measurements of normal stiffness and damping oscillations associated with molecular layering in water,²⁷ OMCTS (Refs. 11 and 13) and TEHOS.⁷ Here, we present simultaneous normal and lateral stiffness measurements, which were performed on TEHOS and OMCTS with Si cantilevers purchased from MikroMasch (Ref. 24) and NT-MDT. TEHOS, purchased from Gelest, Inc,²⁸ is a liquid with nearly spherical and nonpolar molecules (MW=544.97), approximately 1 nm in diameter. The liquid was chosen based on the previous evidence of its layering near solid surfaces as demonstrated by x-ray reflectivity experiments.^{29–31} OMCTS also has nearly spherical molecules of about 1 nm diameter and has been studied intensively in many studies of confined liquids.

In order to illustrate our technique, we simultaneously recorded the cantilever's normal and shear response, A_n and $A_{m,\text{tot}}$ at two well-separated frequencies (dither and shear) upon liquid confinement between the tip and an oxidized, atomically flat Si sample. We used three different cantilevers. Two were unmodified commercial cantilevers and one was modified by FIB to provide improved torsional sensitivity. The planar dimensions were obtained by SEM and we determined the normal stiffness, k_n either by combining geometric methods, measurements of the resonance frequency or fitting of the thermal noise curve.²⁰

For the lever used in Fig. 9, we determined the resonance frequency to be $f = 39.3 \pm 0.02$ kHz, and the length and width were $L = 237.0 \pm 0.9$ μm and $w = 40.7 \pm 0.9$ μm , respectively. The thickness could not be determined from SEM images as it was irregular due to manufacturing flaws. Through fitting the thermal noise²⁰ curve we determined

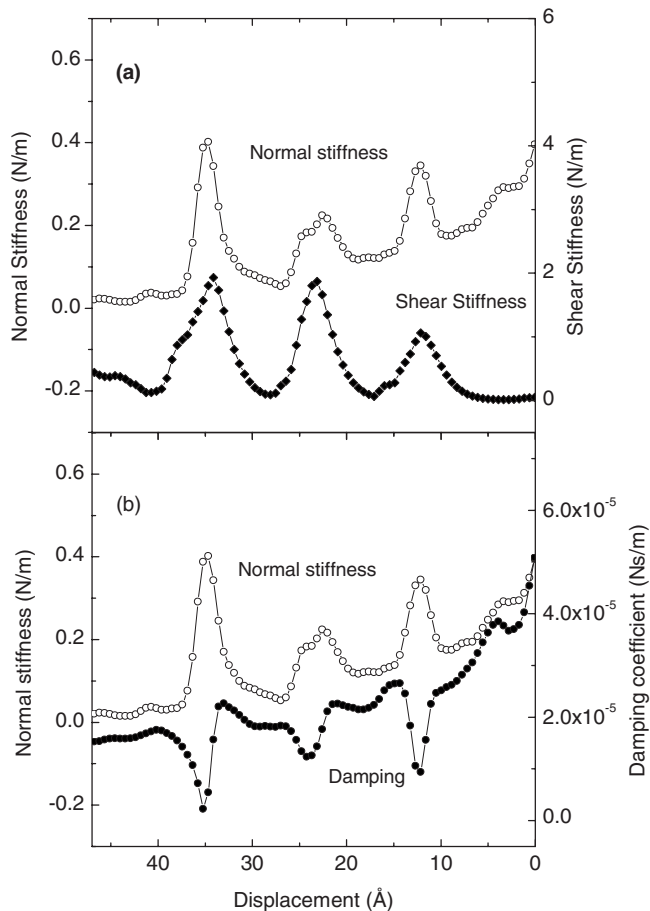


FIG. 10. (a) Normal (open circles) and shear (filled circles) stiffness data of TEHOS confined between the Si substrate and the AFM tip. The oscillations in the shear stiffness are consistent (in phase) with the normal stiffness oscillations. (b) Normal stiffness (open circles) and damping coefficient (filled circles) of TEHOS layers confined between an oxidized, atomically flat Si substrate, and the AFM tip. An average interlayer spacing of 10 Å can be inferred from stiffness and damping oscillations, consistent with the liquid molecular size. The stiffness and damping coefficients are out of phase.

$k_L = 1.73 \pm 0.2$ N/m and by using Eq. (25), we found the effective thickness to be $t = 5.26 \pm 0.76$ μm . For the lateral bending and torsional stiffness, we found $k_b = 103.6 \pm 47$ N/m and $k_t = 85.1 \pm 25$ N/m, respectively. Uncertainties are quite high in this case due to the quality of the thermal fit and the high uncertainty in the lever thickness. Here, we used for Si density $\rho = 2330$ kg/m^3 and $\alpha = 1.8751$.²⁰

The lever used in Fig. 10 was regular and had dimensions of $L = 285 \pm 0.9$ μm , $w = 38 \pm 0.9$ μm , $t = 3.25 \pm 0.25$ μm , and $h = 17.5 \pm 0.9$ μm , while its resonant frequency was experimentally determined, $f = 23.1 \pm 0.02$ kHz. This gave $k_L = 0.42 \pm 0.04$ N/m for this lever, where the 10% error is nearly entirely dominated by gold layer coating and tip corrections. Equations (26) and (27) yielded the lateral bending and torsional stiffness of the beam, $k_b = 57.3 \pm 17.2$ N/m and $k_t = 54.7 \pm 11.0$ N/m, respectively. Here, $\beta = 0.315$ was calculated for a ratio of width to thickness $w/t = 11.69$ (Ref. 23) and the Poisson ratio $\nu = 0.28$ was taken from Ref. 32.

The modified cantilever (Fig. 11) was modified into three sections, but we could not determine its resonance fre-

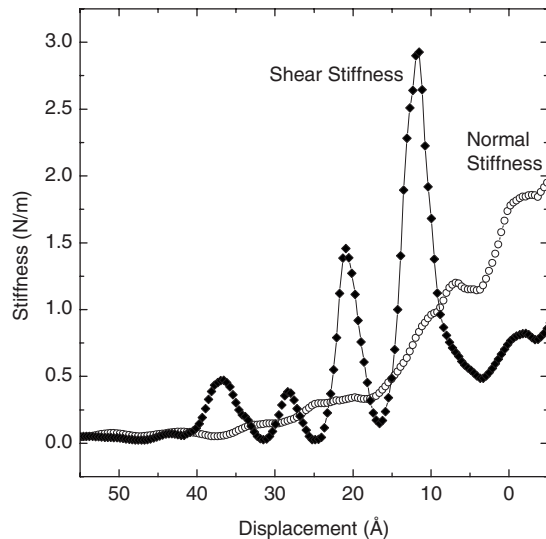


FIG. 11. Simultaneous measurement of the normal and shear stiffnesses of nanoconfined OMCTS using a lever modified for low torsional stiffness. Results are qualitatively quite similar to Fig. 10 obtained with an unmodified lever, but careful alignment.

quencies before it broke during measurement. We did, however, have SEM data of its dimensions and calculated its stiffnesses using the theory provided above, taking $E=150$ GPa. Using Eqs. (30)–(36), we determined $k_L=0.9$ N/m, $k_b=1.5$ N/m, and $k_t=2.3$ N/m. We do not give error bars here as these values depend on six measurements of lever dimensions and uncertainty in the value of E , and therefore the uncertainty in these values is bound to be large. However, these stiffnesses are clearly low enough to provide good separation between normal and lateral measurements.

The sample, an atomically flat piece of Si (100) was oxidized in a Piranha solution (hydrogen peroxide and sulfuric acid 1:3) at 100°C for 20 min, rinsed in de-ionized water, and kept in an oven overnight at 120°C to remove any water traces. The normal stiffness and damping coefficient of the confined liquid layers were obtained by using Eqs. (1) and (2). During our experiments, the fiber was aligned close to the cantilever edge, at a distance of a few micrometers, to enhance the torsional signal sensitivity. The distance from the edge was determined by counting the fiber positioner steps used to reach the measurement position. Once the torsional amplitude was determined via Eq. (21), taking $\delta=0$, the shear stiffness of the confined layers could be calculated from Eq. (8).

IV. RESULTS AND DISCUSSION

Figure 9 shows measurements of the shear stiffness of confined TEHOS (the normal excitation was switched off), both with (filled symbols) and *without* compensation (open symbols). In both cases, the lever edge was visually aligned with the substrate surface to a measured accuracy of $\Delta\epsilon=0.5^\circ$ with the help of a CCD camera with microscope attachment. However, as can be clearly seen, when the compensation circuit is not used, there is a false signal arising from the misalignment between the cantilever surface and

the motion of the shear piezo, i.e., a nonzero $\alpha-\delta$ angle. Comparing to simulations, the misalignment was in $3^\circ-4^\circ$ range. These small misalignments resulted in the curve represented by open symbols, which shows a large apparent shear stiffness far from the surface, which reduces nonphysically close to the surface and then increases again. These artifacts can be suppressed when a compensation circuit is used to align the cantilever motion with the cantilever orientation. By feeding some of the shear signal to the normal (dither piezo), the vector representing the shear motion of the cantilever base can be rotated until the parasitic normal motion is minimized far from the surface (filled symbols). We could reduce the parasitic motion perpendicular to the lever surface to about 0.06 \AA in these measurements, corresponding to a remaining misalignment of about 0.25° . We also found from the simulations that the alignment is in the opposite direction of the lever misalignment (otherwise the measurement would show the artifact shown in Fig. 5-2). This means that we are able to align the cantilever motion within $\beta=0.2^\circ-0.3^\circ$ with respect to the substrate surface. Both measurements show stiffness oscillations with a periods of $10-15\text{ \AA}$, corresponding to the size of the molecules.

Figure 10 shows simultaneous measurements of the normal stiffness, shear stiffness, and damping coefficient of confined TEHOS layers, where the normal and lateral measurements were well separated in the frequency domain as discussed above. These results were obtained with a 5 \AA free vertical (dither) amplitude and a 12 \AA/s approach rate. The lateral amplitude of the cantilever base was $A_{0l}=2.5\text{ \AA}$, while the dither and shear frequencies were 465 Hz and 1.1 kHz , respectively. In this case, we were able to reduce the parasitic normal motion in the shear channel to about 0.01 \AA , due to the smaller shear amplitude used.

In Fig. 10(a) we superimposed the shear stiffness over the normal stiffness data. The two curves show in-phase oscillations revealing that in the ordered, high normal stiffness state, the confined layers are capable of sustaining a shear stress, corresponding to an elastic, solidlike behavior. On the other hand, in the disordered, low normal stiffness state, the shear stiffness is also low suggesting a liquidlike behavior. Even when the normal stiffness rises sharply when the two confining surfaces come very close [right-hand side in Fig. 10(a)], the shear stiffness remains low and nearly constant in the disordered state—a finding that may be of great interest in nanotribology. In Fig. 10(b), the normal stiffness and damping coefficient data show out-of-phase oscillations with a period of 10 \AA that correlate well with the size of TEHOS molecule.

At the used 2.5 \AA shear amplitude, the smallest successfully measured motion normal to the fiber resulting from the torsional motion of the cantilever was 0.016 \AA (corresponding to a measurement of 0.2 N/m in the shear stiffness). Such a small-amplitude measurement is clearly beyond the capabilities of commercial AFMs. In the normal direction, the smallest measured changes in amplitude were of order 0.1 \AA , which falls short of our previously achieved capabilities,²⁷ probably due to the simultaneous measurement of both motions.

Figure 11 shows simultaneous normal and shear mea-

measurements on nanoconfined OMCTS using a FIB modified lever (Fig. 8). Here, the normal amplitude was 1.17 Å and the lateral amplitude was 7.91 Å. As we have learned from Fig. 5, when the torsional stiffness is low, the normal and lateral motions are more effectively decoupled, owing to the much reduced torsional stiffness of the lever. Again, we see oscillations in both the normal and shear stiffnesses with roughly the period of the molecules. These measurements are quite consistent with the measurements on TEHOS, again showing strong oscillations in the shear in the 1–2 N/m range and a low shear stiffness even as the normal stiffness rises sharply. The oscillations in the normal direction are somewhat weaker in this measurement, a feature we have repeatedly observed in these measurements and which we need to explore further.

In conclusion, a new AFM-based technique was developed for simultaneous normal and shear stiffness measurements of confined liquid layers. Although many pioneering experiments have been performed to study the response of confined liquids to a normal or shear stress,^{33–40} the above experiment is, to the best of our knowledge, the first simultaneous measurement of normal and shear stress response of nanoconfined liquids in an atomic force microscope in the linear, small-amplitude regime. This is different from torsional resonance techniques,^{41–44} which have proven quite successful in imaging, but are too disruptive to reveal the molecular-scale structures seen in our study. A very sensitive homebuilt small-amplitude, off-resonance AFM was used to employ the new technique in measurements on TEHOS and OMCTS, liquids with nearly spherical, nonpolar molecules. The results show that both the normal and shear stiffness measurements resolved the layered structure of the confined liquid with an interlayer spacing consistent with its molecular size. We determined optimal conditions to ensure good separation between normal and shear measurements. These include alignment of the cantilever to the substrate, alignment of the cantilever motion using a compensator circuit, low noise measurements of small amplitudes, and reduction of the torsional stiffness through modification of the cantilevers. This work represents a significant advance over our previous AFM measurements performed in confined liquids. It is expected that the development of this technique will improve the understanding of the dynamics of such systems and the stick-slip behavior associated with the sliding of nanoscale films.

ACKNOWLEDGMENTS

J.B.P would like to acknowledge funding by EPSRC (Grant No. GR/L41011/01). P.M.H. would like to acknowledge funding by the National Science Foundation (NSF)(Grant No. DMR-0605900, MRI Grant No. DBI-0321011, ANESA Grant No. INT-0217789, and CAREER Grant No. DMR-0238943), as well as the support of Wayne State University for funding through its Nano@Wayne initiative. We would also like to acknowledge John Mansfield at EMAL, University of Michigan for assistance with the Focused Ion Beam modifications.

- ¹B. Bushan, J. N. Israelachvili, and U. Landman, *Nature (London)* **374**, 607 (1995).
- ²J. N. Israelachvili and P. M. McGuiggan, *Science* **241**, 795 (1988).
- ³S. Granick, *Science* **253**, 1374 (1991).
- ⁴S. J. O'Shea, M. E. Welland, and J. B. Pethica, *Chem. Phys. Lett.* **223**, 336 (1994).
- ⁵M. Heuberger, M. Zach, and N. D. Spencer, *Science* **292**, 905 (2001).
- ⁶A. Mukhopadhyay, J. Zhao, S. C. Bae, and S. Granick, *Phys. Rev. Lett.* **89**, 136103 (2002).
- ⁷S. Patil, G. Matei, C. A. Grabowski, P. M. Hoffmann, and A. Mukhopadhyay, *Langmuir* **23**, 4988 (2007).
- ⁸J. Gao, W. D. Luedtke, and U. Landman, *Phys. Rev. Lett.* **79**, 705 (1997).
- ⁹E. Kumacheva and J. Klein, *Science* **269**, 5225 (1995); J. Klein and E. Kumacheva, *J. Chem. Phys.* **108**, 6996 (1998).
- ¹⁰A. L. Demirel and S. Granick, *Phys. Rev. Lett.* **77**, 2261 (1996); A. L. Demirel and S. Granick, *J. Chem. Phys.* **115**, 1498 (2001).
- ¹¹S. Patil, G. Matei, A. Oral, and P. M. Hoffmann, *Langmuir* **22**, 6485 (2006).
- ¹²A. Oral, R. A. Grimble, H. Ö. Ozer, and J. B. Pethica, *Rev. Sci. Instrum.* **74**, 3656 (2003).
- ¹³S. Patil, G. Matei, H. Dong, P. M. Hoffmann, M. Karaköse, and A. Oral, *Rev. Sci. Instrum.* **76**, 103705 (2005).
- ¹⁴P. M. Hoffmann, *Appl. Surf. Sci.* **210**, 140 (2003).
- ¹⁵P. M. Hoffmann, *Small-Amplitude Atomic Force Microscopy in Dekker Encyclopedia of Nanotechnology* (Dekker, New York, 2004), p. 3641.
- ¹⁶D. Rugar, H. J. Mamin, and P. Guethner, *Appl. Phys. Lett.* **55**, 2588 (1989).
- ¹⁷R. J. Clarke, O. E. Jensen, J. Billingham, A. P. Pearson, and P. M. Williams, *Phys. Rev. Lett.* **96**, 050801 (2006).
- ¹⁸T.-D. Li, J. Gao, R. Szoszkiewicz, U. Landman, and E. Riedo, *Phys. Rev. B* **75**, 115415 (2007).
- ¹⁹N. Burnham, X. Chen, C. S. Hodges, G. Matei, E. J. Tjoreson, C. J. Roberts, M. C. Davies, and J. B. Tandler, *Nanotechnology* **14**, 1 (2003).
- ²⁰G. Matei, E. J. Thoreson, J. R. Pratt, D. B. Newell, and N. A. Burnham, *Rev. Sci. Instrum.* **77**, 083703 (2006).
- ²¹O. Piétrement, J. L. Beaudoin, and M. Troyon, *Tribol. Lett.* **7**, 213 (1999).
- ²²S. P. Timoshenko and J. N. Goodier, *Theory of Elasticity*, 3rd ed. (McGraw-Hill, New York, 1970), Chap. 10.
- ²³V. D. daSilva, *Mechanics and Strength of Materials* (Springer, Berlin, 2006), Chaps. 9 and 10.
- ²⁴Cantilevers from MicroMasch, 7086 SW Beveland Road, Portland, OR.
- ²⁵S. P. Jarvis, H. Tokumoto, H. Yamada, K. Kobayashi, and A. Toda, *Appl. Phys. Lett.* **75**, 3883 (1999).
- ²⁶Y. Song and B. Bhushan, *J. Appl. Phys.* **99**, 094911 (2006).
- ²⁷S. Jeffery, P. M. Hoffmann, J. B. Pethica, C. Ramanujan, H. Ö. Ozer, and A. Oral, *Phys. Rev. B* **70**, 054114 (2004).
- ²⁸Gelest, Inc., 11 Steel Road East, Morrisville, PA.
- ²⁹C. J. Yu, A. J. Richter, A. Dutta, M. K. Durbin, and P. Dutta, *Phys. Rev. Lett.* **82**, 2326 (1999).
- ³⁰C. J. Yu, G. Evmenko, J. Kmetko, and P. Dutta, *Langmuir* **19**, 9558 (2003).
- ³¹C. J. Yu, G. Evmenko, A. G. Richter, A. Dutta, J. Kmetko, and P. Dutta, *Appl. Surf. Sci.* **182**, 231 (2001).
- ³²T. Dobrek, R. W. Stark, and W. M. Heck, *Phys. Rev. B* **64**, 045401 (2001).
- ³³R. G. Horn and J. N. Israelachvili, *J. Chem. Phys.* **75**, 1400 (1981).
- ³⁴J. P. Cleveland, T. E. Schäffer, and P. K. Hansma, *Phys. Rev. B* **52**, R8692 (1995).
- ³⁵A. Dhinojwala and S. Granick, *J. Am. Chem. Soc.* **119**, 241 (1997).
- ³⁶W. Han and S. M. Lindsay, *Appl. Phys. Lett.* **72**, 1656 (1998).
- ³⁷S. P. Jarvis, T. Uchihashi, T. Ishida, H. Tokumoto, and Y. Nakayama, *J. Phys. Chem. B* **104**, 6091 (2000).
- ³⁸M. Antognozzi, A. D. L. Humphris, and J. Miles, *Appl. Phys. Lett.* **78**, 300 (2001).
- ³⁹S. J. O'Shea, *J. Appl. Phys.* **40**, 4309 (2001).
- ⁴⁰A. L. Demirel and S. Granick, *J. Chem. Phys.* **115**, 1498 (2001).
- ⁴¹T. Kawagishi, A. Kato, Y. Hoshi, and H. Kawakatsu, *Ultramicroscopy* **91**, 37 (2002).
- ⁴²L. Huang and C. Su, *Ultramicroscopy* **100**, 277 (2004).
- ⁴³M. Reinstädter, T. Kasai, U. Rabe, B. Bhushan, and W. Arnold, *J. Phys. D* **38**, R269 (2005).
- ⁴⁴T. Kunstmann, A. Schlarb, M. Fendrich, D. Paulkowski, Th. Wagner, and R. Miller, *Appl. Phys. Lett.* **88**, 153112 (2006).